Chemical Reactions as a Means of Installing Adlayers on Electron Transport Layers

Kevin C. DePope[a], Siliang He[b], Yicheng Liu[b], Evgeny Pakhomenko[b], Russell J. Holmes[b], and Jacob W. Ciszek[a*]

[a]Loyola University Chicago, 1068 W. Sheridan Road, Chicago, IL 60660, USA. Email: jciszek@luc.edu

[b]Department of Chemical Engineering and Materials Science, 421 Washington Ave. SE, Minneapolis, MN 55455, USA.

Abstract

Adlayers are often placed at metal-on-organic interfaces as a common strategy to alleviate damage during metal deposition by thermal evaporation. Methods of chemically installing adlayers have been recently demonstrated on organic semiconductors that address these interfacial issues while providing many secondary benefits. Chemical installation has yet to be attempted at the cathode-electron transport layer (ETL) interface within organic light-emitting devices (OLEDs), offering a powerful option to optimize electron injection, improve surface wetting, and reduce metal penetration. Here, a reaction between TPBi (2,2',2"-(1,2,5-benzinetriyl)-tris(1-phenyl-1-H-benzimidazole) and propylene oxide results in a controllable 1-3 nm thick layer of propylene oxide as shown by high-resolution X-ray photoelectron spectroscopy (XPS) and energy dispersive X-ray spectroscopy (EDX). The reactive addition of the adlayer at temperatures below 40 does not affect the morphology of the thin film and reaches a high degree of coverage within 3 hours. Integration of this layer into a phosphorescent OLED does not introduce any significant negative impact on device function. This result opens up the possibility of introducing further specific functionality into the adlayer to engineer OLED performance.

Keywords

Adlayer, Metal-Organic Interface, Electron Transport Layer (ETL), TPBi, OLEDs

1. Introduction

The deposition of a metal onto a soft organic thin film within an OLED to form a cathode comes with particular challenges. High energy and unbound metals penetrating the organic layers can increase leakage current [1,2], affect light emission through plasmonic or non-radiative quenching effects [3], and cause bright spots to appear on the active area [4]. Metalation also damages the organic, creating trap states, lowering electron injection, and reducing device efficacy and light output over time [5]. Other flaws include thermal damage, aggregation of metal on the surface, and poor metal stability [6–9]. These, in part, stem from high energy metal impinging on the surface of the ETL, while the low interactions of the ETL for the metal layer allow penetration/diffusion [10].

One method to address these problems is to insert an adlayer between the metal-on-organic interface, which is especially prominent with OPVs and to a lesser extent in OLEDs.

These adlayers can be comprised of inorganic dielectrics (CsCl, Si_2O etc.) [11], metals/metal oxides (TiO_x, Al_2O_3 CrO_x, etc.)[12], mixed polymer interlayers (P3HT, PEDOT:PSS, PMMA, etc.)[13,14], and organic buffers (CuPc, PCBM, etc.) [15] between the organic material and metal contact. The adlayers first serve as a blocking layer mitigating the damage/penetration of the thermally evaporated metals [10,16] and then further provide better adherence [17] which can limit post-deposition diffusion. The adlayers often have additional advantages, such as reducing injection barriers [18] or secondary functions like an oxidative/degradation-resistant layer [19,20]. Research into different methods of installing interlayers sought to avoid the challenges seen with thermal deposition of adlayers by instead utilizing metal oxide solution processing [12], atomic layer deposition of metal oxides or noble metals [21], and low temperature thermal evaporation of organic interlayers [15]. However, there are significant challenges that arise from the utilization of these types of techniques. Spin-coated solution-processed layers are hindered by rough surface morphologies and the solvents could wear away or dissolve the organic surface [22,23]. Atomic layer deposition (ALD) has limited metal selection, unintended by-products that incorporate with growth materials and can be subjected to decomposition [21].

An alternative method of installing adlayers is through a chemical reaction. This addresses most of the aforementioned challenges while providing additional potential benefits. Specifically, chemical modification can be designed to install a high surface coverage of functional groups that are affixed to the surface. Additionally, adlayer chemistry can be installed with a high degree of control over thickness (e.g. 1-3 nm), offers diverse functionality or multiplexing, and can target low temperatures avoiding decomposition associated with thermal deposition [24]. Previous reactions have been shown to work on organic semiconductors but not on common ETLs [25,26]; as such, work is needed to demonstrate the viability of chemical installation of an adlayer on an ETL. This is *especially* true as the reaction must not negatively affect the sensitive OLED emissive layer for this approach to offer another means of modification.

Herein, we demonstrate the reaction of propylene oxide with the archetypical ETL 2,2',2"-(1,2,5-benzinetriyl)-tris(1-phenyl-1-H-benzimidazole) (TPBi) as a means of chemically installing adlayers on the surface. We demonstrate that treatment of TPBi under varying conditions leads to a controllable addition of propylene oxide on the organic surface. The ability to maintain a continuous thin-film under reactive conditions is probed, while adsorption/mechanistic studies can be used to justify both the mode of bonding and adlayer structure. In accordance with application in OLEDs, the reaction is probed for its compatibility with device stacks.

2. Methods

2.1 Materials

TPBi (≥99.5%, sublimed grade) was obtained from Sigma-Aldrich while evaporation metals (Cr and Au) were of >99.9% purity and purchased from Kurt J. Lesker. Reagent grade propylene oxide (≥99%) from Sigma-Aldrich was used. Organic materials 4,4',4-tris(carbazol-9-yl)triphenylamine (TCTA), 4,4'-bis(carbazol-9-yl)biphenyl (CBP), tris(2-phenylpyridine)iridium ($Ir(ppy)_3$) (>99.5%, sublimed grade) were purchased from Luminescence technology corp. and

used as received. Molybdenum (VI) oxide (>99.5%, ACS grade) was purchased from Alpha Aesar and used as received.

2.2 TPBi Thin Film Preparation

Microscope slides were cut (12×25×1 mm) and cleaned with piranha solution (3:1, H_2SO_4:H_2O_2) for 30 min. The slides were washed with deionized water, sonicated in isopropyl alcohol for 15 min, and dried with a stream of nitrogen. For gold slides, the cut and cleaned glass was placed in a thermal evaporator (Kurt J. Lesker NANO38) and 5 nm of Cr followed by 100 nm of Au were deposited at a rate of 1 Å/s at a base pressure of 9×10^{-7} torr. 30 nm of TPBi was then sublimed onto fresh gold or cleaned glass slides at a rate of 1.0 Å/s in a custom sublimation chamber with a source to sample distance of 16–17.5 cm (<8.0×10^{-6} torr base pressure).

2.3 Reaction of Thin-Film TPBi with Propylene Oxide

Freshly sublimed TPBi slides were placed at the far end of a sealed tube (100 mL) with a 2 mL vial on the opposite end, nearest a septum. The tube was evacuated and filled with nitrogen three times. Propylene oxide was injected into the vial (which served as the reservoir) through the septum The septum was replaced with a screw cap and the sealed tube was left under nitrogen for the duration of reaction. Reaction time, temperature, and reactant amounts are specified in the text.

2.4 Morphology Assessment Using SEM and Extent of Reaction Using SEM-EDX

The surface morphology before and after reactions was examined at room temperature using SEM imaging on a Hitachi SU3500 microscope. The samples were mounted onto a specimen stub using carbon double-sided conductive tape where scans using an acceleration voltage between 3.0-5.0 kV for secondary electron (SE) images were taken. Backscatter images (BSE-COMP) were taken at the same acceleration voltages and processed in ImageJ. Images were processed using a binary threshold differentiating substrate (light areas) from carbon (dark areas). Relative areas were calculated to determine TPBi coverage. Elemental composition measurements were taken for 45 seconds using 1.0 kV, 100 spot intensity, and 400× magnification using a Bruker Xflash 6-30 energy-dispersive X-ray (EDX) detector and used to determine the extent of the reaction.

2.5 Thin Film and Adlayer Thickness Determination Using Ellipsometry

Freshly deposited gold slides were quickly placed onto the stage of a Gaertner Stokes LSE Ellipsometer to obtain the extinction coefficient and refractive index measurements of the gold slide. TPBi thickness was obtained after deposition using the refractive index of 1.73 giving the exact film thickness. The sample was then reacted with propylene oxide and the thickness was measured again using a refractive index of 1.36 for the chemically installed adlayer.

2.6 Characterization of Thin Film Reaction using High-Resolution XPS

High-resolution carbon (C 1s), oxygen (O 1s), and nitrogen (N 1s) XPS scans were taken using a Kratos Axis-165 with a monochromatic Al Kα (1486.6 eV) X-ray source. The X-ray had a spot size of 400 μm, 10 mA emission, 20 eV pass energy, a 0.1 step size, and 0.45 eV energy resolution. A 180-degree, 165 mm hemispherical analyzer was utilized at a take-off angle of 90 degrees. XPSPEAK4.1 software was used for peak fitting using a 30:70 ratio Lorentzian-Gaussian function with no varying line widths and a Shirley background. The spectra were referenced using the nitrogen signal, shifting the N 1s peaks to 398.9 eV [27–29].

2.7 Contact Angle Measurement

A 30 nm TPBi film was prepared on gold coated glass slides. Half the samples were reacted for 3 h at 37 . Reacted and unreacted samples were placed onto a sample stage in front of a fixed camera where a 15 μL drop of 18.2 MΩ-cm water was placed on the surface and images were taken. Tangent lines were manually drawn and contact angles manually measured.

2.8 OLED Fabrication and Reaction

OLEDs were fabricated on organic substrates pre-coated with a 130 nm-thick layer of indium-tin-oxide (ITO; Kintec) with a sheet resistance of 15 Ω/□. Prior to organic film deposition, substrates were washed with tergitol solution (Sigma-Aldrich) followed by deionized water. Next, the substrates were sonicated in acetone for 10 min, cleaned with boiling isopropyl alcohol for 10 min, and treated with UV-ozone ambient for 15 min. Organic layers were deposited in a thermal evaporator (Angstrom Engineering EvoVac) at 1-2 Å/s with a base pressure of $< 9\times10^{-7}$ torr. The Al cathode was deposited at a rate of 2.5 Å/s through a shadow mask, defining a device active area of 4 mm^2. The device stack had the following structure: ITO / TCTA: MoO_3 (150 nm, 9 vol%) / TCTA (20 nm) / CBP: $Ir(ppy)_3$ (10 nm, 7 vol %) / TPBi (60 nm) / LiF (1 nm) / Al (100 nm). After fabrication was completed, the device was encapsulated with epoxy and a glass cover in an N_2 glovebox. For the reaction, after the TPBi layer was deposited, the stack was removed from the evaporator and reacted with 10.0 μL of propylene oxide for 3 h at 37 . Control devices were left under the N_2 environment during the reaction.

3. Results and Discussion

The reaction between propylene oxide and TPBi was inspired by prior solution-phase experiments where propylene oxide was added to several monosubstituted imidazoles [30,31], adding to the nitrogen at the 3 position (light blue circle in Figure 1a). The reaction was adapted to the solid phase and applied to a 30 nm thick film of TPBi, whereby the film was exposed to vapor phase propylene oxide in an inert environment. Figure 1 shows the proposed solid phase reaction with the addition of propylene oxide to the benzimidazole groups of TPBi with up to three reaction sites available. Similar vapor/solid reactions (small molecule adsorbates with pentacene/tetracene) are known to occur primarily at the surface, leading to the proposed adlayer structure [26,32]. The addition of an oxygenated species allows for a spectroscopic marker of

reaction that also has functional application, e.g. reducing metal penetration from thermal deposition of the cathode [32].

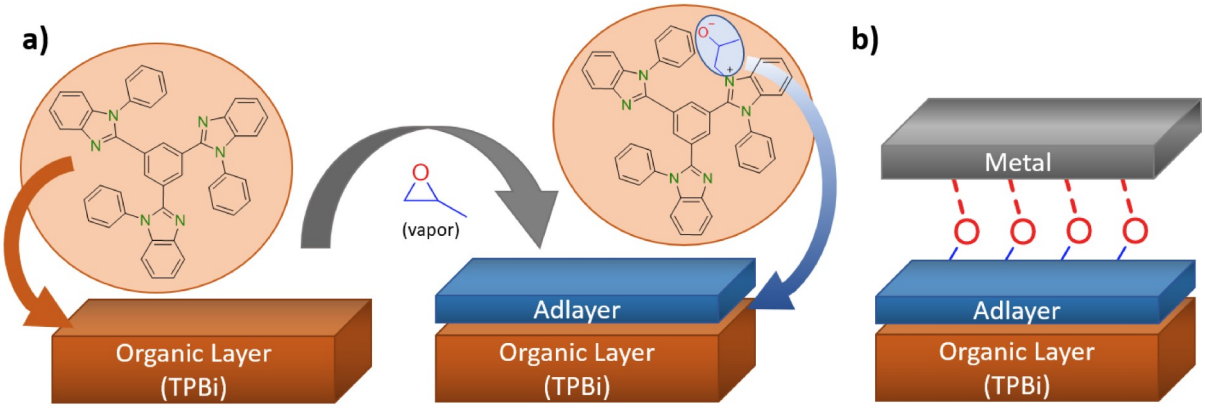

Figure 1. (a) Adlayer formation on the surface of thin-film TPBi during solid-vapor phase chemical reaction with propylene oxide. (b) Potential metal-organic interactions of the propylene oxide adlayer.

XPS was used to characterize the reactions due to its surface sensitivity and ability to determine atomic composition and oxidative states of elements [33]. In particular, increased levels of oxygen on TPBi will indicate a potential reaction. Figure 2 shows the high-resolution XPS spectra of the O 1s, C 1s, and N 1s regions of both unreacted and reacted TPBi. In the O 1s region, there is a significant increase in oxygen percent to 3.6% (increase of 1.7%) for the reacted samples indicating adlayer formation. This level of oxygen represents a fully formed adlayer across the surface, rather than a low-density addition at a single location on the TPBi such as depicted in the inset of Figure 1a.

The C 1s region should give an indication of the differences in chemical state after the reaction. Figure 2b shows TPBi both pre- and post-reaction, with a notable shoulder appearing at a higher binding energy region after 3 h exposure to propylene oxide. Assessment of the changes to the film is accomplished by deconvolution of the two measurements. Deconvolution of the control is accomplished by fitting to two peaks corresponding to the C-C and C-N bonds at 285.1 and 286.0 eV respectively [28]. The ratio between the C-C to C-N peaks is 2.7 to 1, which also reflects expected ratios in TPBi ($C_{44}N_6H_{22}$, 33 C-C, 12 C-N). After the reaction, the C 1s peak significantly shifts towards oxygenated carbon (>286 eV) as well as the added intensity of C-N, consistent with the proposed reacted structure. Figure 2c shows this deconvolution for reacted TPBi and, keeping the same assignments for C-C and C-N, the relative amount of C-N increases to 2.4 to 1, indicating additional C-N bonds are being formed when propylene oxide is added to the imidazole. Additionally, two new peaks were needed at 286.2 and 286.7 eV which correspond to reported $C\text{-}N^+$ [27,29] and expected C-O binding energies. The $C\text{-}N^+$ peak is small and appears 0.2 eV higher than the uncharged C-N and its addition significantly improves the deconvolution, while the $C\text{-}O^-$ only minimally improves curve fitting but is necessary for elemental consistency with the O 1s measurements.

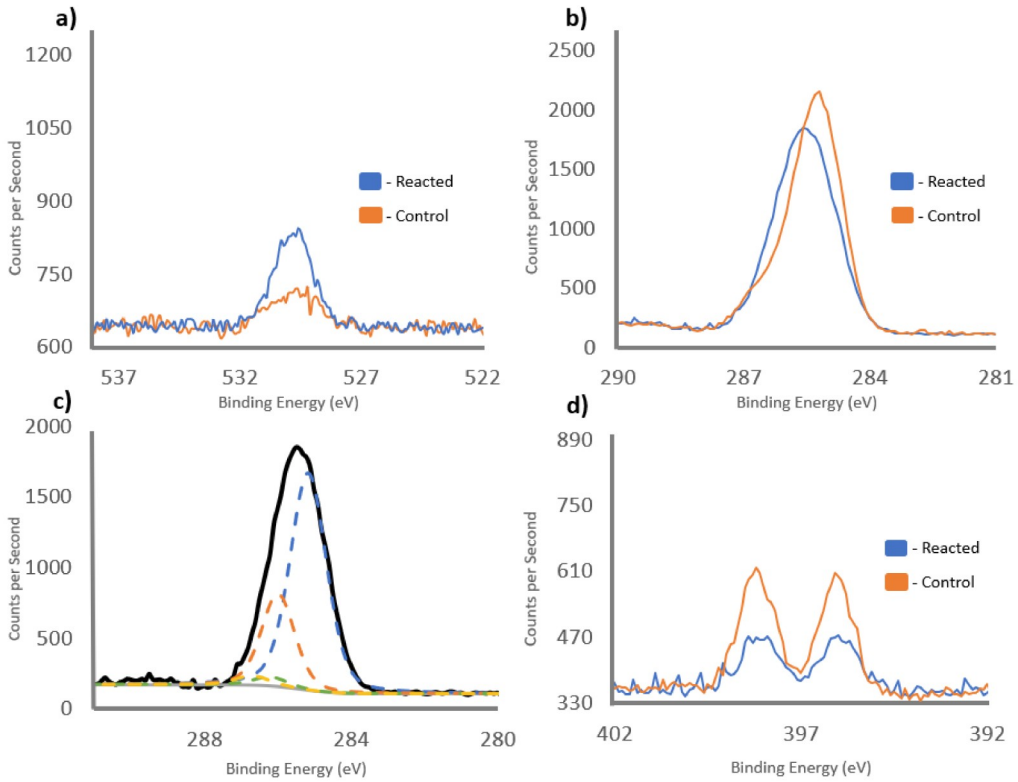

Figure 2. High-resolution XPS spectra of the (a) O 1s region and (b) C 1s region. (c) Deconvolution of the C 1s signal for the reacted sample. Signals are as follows C-C blue, C-N orange, C-N^+ green, C-O yellow, raw signal in black, and background in grey (d) High-resolution XPS spectra of the N 1s region. Blue spectra correspond to the reacted sample. Orange spectra correspond to the unreacted sample.

The N 1s region also provides data, namely the signal decreases after the reaction, which can be used to confirm the location and coverage of the installed adlayer. In the case of an adlayer covering the surface of TPBi, any photoelectrons generated from the underlying TPBi are now attenuated, decreasing the observed intensity. This is consistent with the measured data which contains a 45% decrease in the N 1s signal pre- to post-reaction, and thus is the basis of the proposed structure. Moreover, this decrease can be used to calculate the adlayer thickness. Here, the intensity from unreacted samples can be used to establish the XPS normalization factor which, along with parameters such as the mean free path of an electron and approximate atom density, allow for the thickness to be determined [34,35]. These calculations (Eq. 1-3 in SI) measure an attenuating adlayer thickness of roughly 1 nm. Again, a full discussion of coverage occurs during mechanistic studies (vide infra), but the thickness is slightly larger than the molecular length of propylene oxide on a surface (~0.4 nm), suggesting the adlayer might be two to three molecules thick. Peak fitting of the N 1s of the reacted sample, seen in Figure S1, show a new peak corresponding to a nitrogen cation and a decrease the sp^2 hybridized nitrogen signal consistent with the hypothesized reaction. Regardless, the increase in oxygen, presence of the adlayer, and stability of composition under ultra-high vacuum conditions (<10^{-8} Torr) are all indicative of a successful reaction on the surface of TPBi.

To further corroborate the reaction, EDX was used in conjunction with additional controls. At low accelerating voltages, EDX provides similar composition information and depth sampling to XPS but also allows for the rapid screening necessary for condition optimization. The first set of measurements, shown in Figure 3a, are the controls used to corroborate the reaction. The thin film TPBi was exposed to heat as a negative control and then to ethyl ether as a non-reactive oxygenated species to eliminate the possibility of non-reactive adsorption. As expected, the exposure to the control conditions yielded no significant increase in oxygen percentage with the controls both measuring at 1.0%, near the background signal for freshly deposited TPBi. In contrast, exposure to propylene oxide significantly increased the oxygen percentage to 1.6%. The increase in oxygen due to propylene oxide exposure over the controls supports the conclusion from XPS that the oxygen presence and adlayer formation is due to new bond formation, between substrate and reactant.

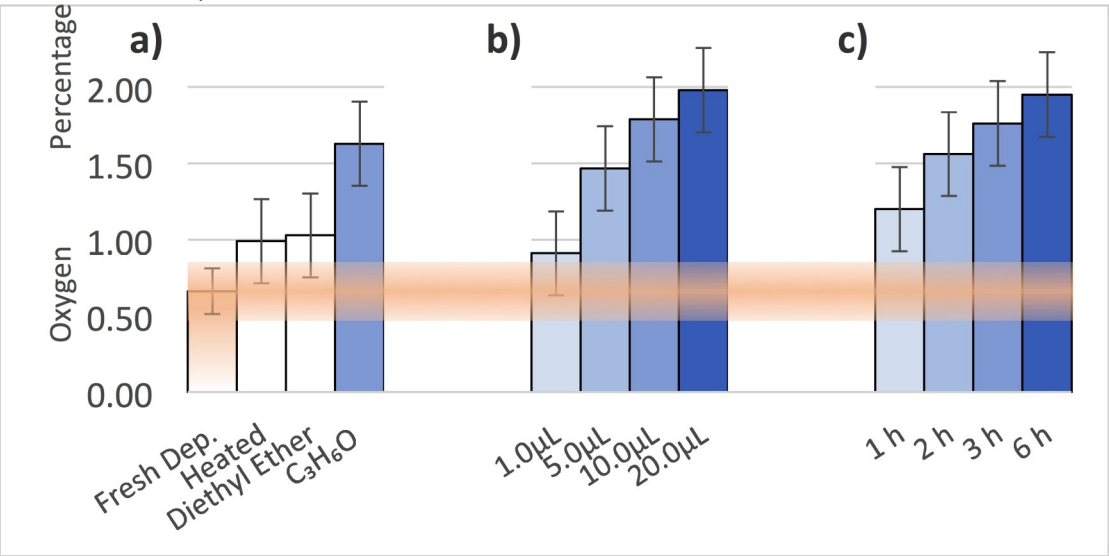

Figure 3. Relative oxygen percentages obtained by EDX. (a) Propylene oxide (C_3H_6O) reaction versus three controls of freshly deposited TPBi, TPBi *only* heated 37 for 3 h (no reactant), and TPBi exposed to diethyl ether all at 37 for 3 h. (b) Increasing the concentration of propylene oxide from 1.0 to 20 µL at 37 for 3 h. (c) Increasing the time from 1 to 6 h at 37 and 10 µL of propylene oxide.

With the efficacy of the reaction corroborated, reaction conditions were optimized. Figure 3b shows the measured oxygen percentage of TPBi, exposed to increasing concentrations of propylene oxide, to determine its effect on reaction at 3 hours of exposure. Low amounts of propylene oxide (1.0 µL) result in virtually no increase in oxygen percentage at 0.9%, similar to the control oxygen percentages shown previously. Larger additions (5.0, 10.0, and 20.0 µL) result in the expected dependence of reactivity on concentration with the oxygen percentage increasing to 1.5, 1.8, and 2.0% respectively. Larger concentrations become incompatible with the formation of quality adlayers, as described below, while 10 µL is near ideal for the time, temperature, and chamber volume used.

Varied reaction times were also considered. Figure 3c shows that reaction durations > 1 h were needed to obtain a statistically significant increase in oxygen percentage. Longer durations

(2, 3, and 6 h) result in the expected dependence on time, with oxygen percentages increasing to 1.6, 1.8, and 2.0% respectively. It is important to briefly note that these changes in composition are also accompanied by associated thickness increases. Ellipsometry measurements, shown in the supporting information Table S1 and Table S2, were taken of the reacted samples show that 3-hour reactions result in layers between 1.3 and 2.2 nm thick layers slightly thicker than the values measured by XPS. A maximum of 3.3 nm is observed when the reaction is extended to 6 hours.

Though reaction condition ranges have been examined, there is still one critical variable to consider: TPBi films have a propensity to crystallize This process is known to occur under heating [36,37] and could potentially be accelerated by added media (i.e. propylene oxide). Heated systems can also form non-continuous films as a result of crystallization, which would be incompatible with devices. Accordingly, scanning electron microscopy (SEM) was used to determine reaction conditions conducive to maintaining a continuous thin film. Figure 4a shows an illustrative TPBi film from non-viable conditions (100 nm film of TPBi, 10 μL of propylene oxide at 80 for 6 h) and microscopy images display distinct contrast between the areas covered with TPBi (dark) and the exposed gold substrate (light). Generally, the appearance of crystalline dendritic morphology features is accompanied by an exposed substrate, as is the case in Figure 4a. The average coverage of TPBi under those conditions was determined using backscatter images and was 52 ± 8% (Figure S2). Numerous conditions were screened to minimize the appearance of these features and maximize the continuity of the TPBi, including time, temperature, and substrate. The substrate material has a fairly significant influence on maintaining a continuous thin film, as seen in Figure S3. *TPBi deposited on top of an organic material maintains a more consistent coverage after heating, followed by silicon and then gold*. It has also been demonstrated that reducing film thickness reduces TPBi's ability to form crystallization fronts while reducing temperature limits crystal growth rate [36]. Reducing film thickness (30 nm), reaction temperature (≤ 40), and time (< 3 h) were effective in minimizing the formation of non-continuous dendritic features. For example, although a 30 nm film treated with 10 μL of propylene oxide for 6 h at 37 contains a significant amount of crystalline-like material (Figure 4b, on the left and right of the image), a continuous film of TPBi starts to emerge, seen by the uninterrupted dark grey area in the center. When the reaction time is reduced to 3 hours, a continuous film, absent of any dominant crystalline-like features, is retained (Figure 4c). Further examples of time-dependence annealing are shown in SI (Figure S4). Finally, using higher amounts of reactant or temperatures lower than the boiling point of the reactant leads to wetting of the surface as seen in Figure 4d. Under these conditions we presume that the reactant has aggregated on the surface of the TPBi, dissolving the organic film and, once dried, leaves isolated clusters of TPBi on the surface. Therefore, reactions at 37 for 3 hours with 10.0 μL of propylene oxide on thinner films (<50 nm) are optimal to maintain thin film integrity compatible with devices while maximizing the amount of oxygen on the surface.

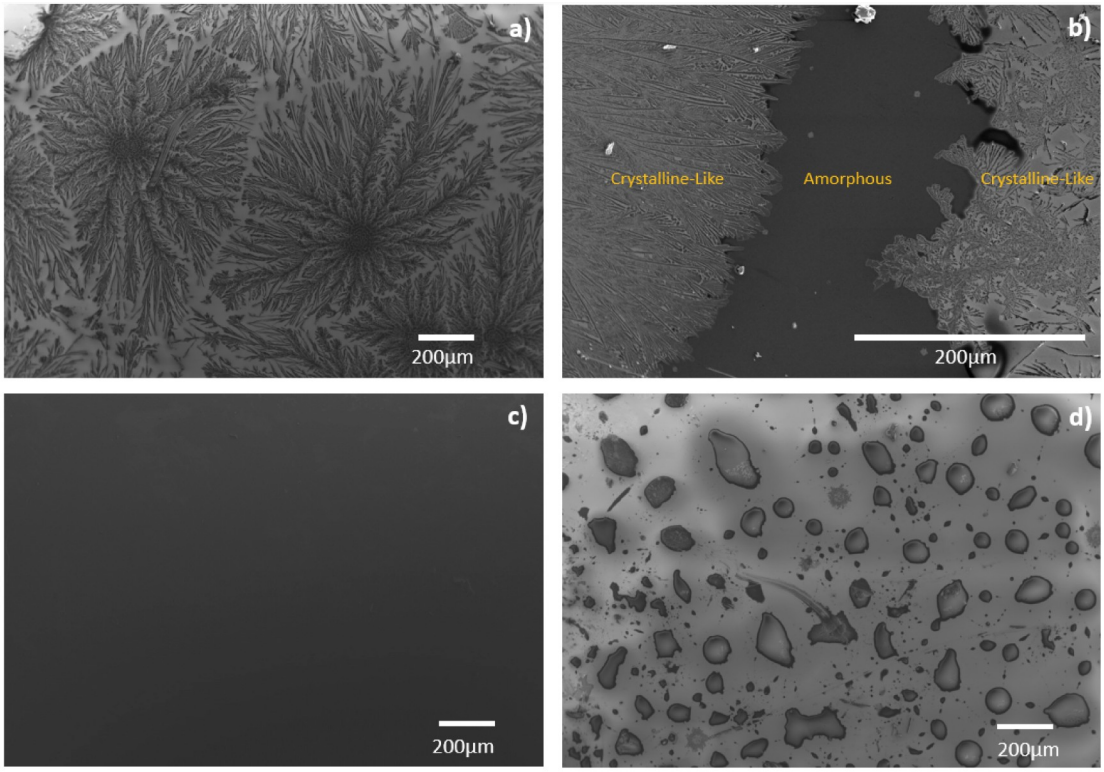

Figure 4. (a) SEM image of a 100 nm thick film of TPBi heated at 80 for 6 h with 10 µL of propylene oxide showing significant annealing of TPBi (dark) and exposed gold substrate (light). (b) SEM image of 30 nm of TPBi heated 37 for 6 h with 10 µL of propylene oxide showing continuous thin film character starting to emerge in the center of the film. (c) SEM image of 30 nm of TPBi reacted at 37 for 3 h with 10 µL of propylene oxide maintains a continuous thin film on the surface. (d) SEM images of 30 nm TPBi reacted at 37 for 3 h with 20.0 µL propylene oxide where TPBi appears in localized clusters with large gaps of substrate between them. Secondary electron images were taken at an acceleration voltage of 3.0 kV.

With the reaction conditions optimized, our analysis shifted to the mechanistic aspects of the reaction. Upon reanalyzing the C 1s deconvolution, we first find that XPS data is consistent, though not definitive, with the reaction forming a ring-opening product, which we presume to be our first step of the reaction. This step is also consistent with prior solution phase work on unsubstituted and monosubstituted imidazoles [30]. The remaining data heavily suggest a subsequent step to occur. XPS and ellipsometry data show an adlayer with a calculated thickness of ~1 nm at 3 hours. This is notably greater than the molecular length of propylene oxide (~0.4 nm). Thicknesses determined via ellipsometry also continue to increase well past this length with extended reaction times. This suggested a mechanism whereby the initial reaction occurs at the nitrogen of the imidazole, then later vaporous propylene oxide can react with this adsorbed species, leading to multiple adsorptions or oligomerization. This mechanism is also based on solution phase precedence where propylene oxide has been observed to undergo polymerization under certain conditions [38]. We looked for additional evidence of this mechanism at high temperatures/times. Though these conditions would sacrifice overall film integrity, the higher degree of reaction would allow for easier analysis because of the thicker adlayers.

Using high-resolution XPS of films reacted at 80 , we found that there was significantly more attenuation of the N 1s signal, thus the higher thicknesses measured by ellipsometry were corroborated in XPS (Figure S5). However, the primary goal was to isolate the signal from the propylene oxide adlayer, which was accomplished by subtracting the subsurface TPBi signal. The nitrogen signal (only present in TPBi) has a fixed 6:45 ratio to carbon. Using the nitrogen signal to determine the amount of carbon associated with subsurface TPBi, the bulk TPBi signal can be separated from the adlayer, as shown in Table 1. Accordingly, 57.6% of the carbon signal was assigned to the bulk and was subtracted from the reacted XPS measurements, meaning 28.1% C and 7.9% O are attributed to the adlayer. This is equivalent to a carbon-to-oxygen ratio of 3.4 to 1 and is close to the 3 to 1 of propylene oxide indicating propylene oxide is the only material responsible for what is happening on the surface. Coupled together, the data appears consistent with a mechanism based on the initial reaction with TPBi in the initial 1-2 hours, followed by a transition to oligomerization at >3 hours, higher temperatures, or higher concentrations.

Table 1. Isolation of Adlayer Signal from High-Temperature TPBi and Propylene Oxide Reaction (80)

	TPBi Composition	Reacted XPS Signal	Signal Attributed to TPBi Subsurface	Signal Attributed to Adlayer	Adlayer Ratio
Carbon	88.2	84.4	57.6	28.1	3.4
Nitrogen	11.8	7.7	7.7		
Oxygen		7.9		7.9	1

With confirmation of adlayer formation, it was important to determine if the adlayer could alter the surface properties of the TPBi thin film. This was examined two ways. First, contact angle measurements were performed to assess whether surface wettability could be increased via to the propylene oxide adlayer. Before reaction, a freshly deposited 30 nm TPBi thin film had a contact angle of averaging 76 ±3°, shown in Figure 5a. After reaction, the TPBi film displayed a lower contact angle, averaging 66 ±3° (Figure 5b). Thus, the appended adlayer does impact the surface properties. The second experiment examined whether the propylene oxide adlayer would limit crystalline-like feature formation after installation. Overall, TPBi is known to be less prone to annealing after deposition of additional layer. We find that after reaction, a TPBi thin film with an adlayer developed less crystalline-like features then pristine TPBi when both were exposed to heat (40 °C for 3 h). More than 50% of pristine TPBi samples showed appreciable dendritic features (>30% of surface) after heating, while surfaces containing adlayers never showed any increase in dendritic features (12 samples), Figure S6. Combined, the two experiments demonstrate the potential of adlayers to impact surface properties of TPBi.

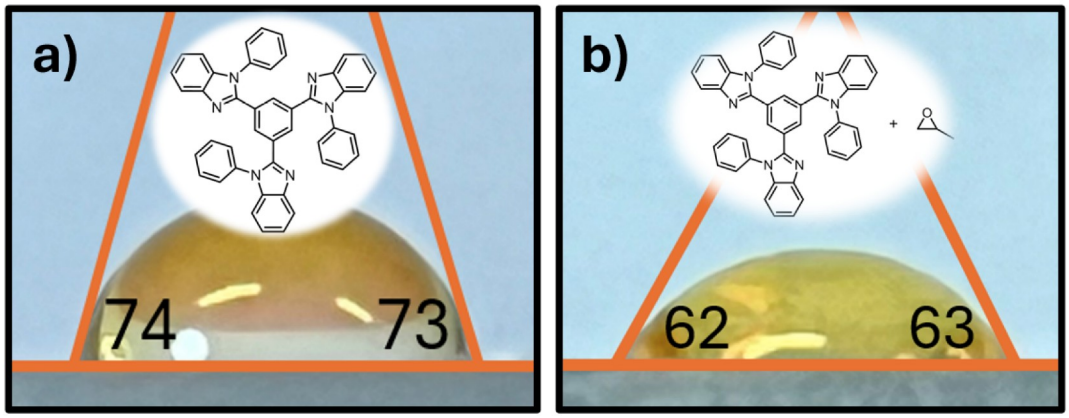

Figure 5. Image of a water droplet on (a) unreacted and (b) reacted thin films of TPBi, used to measure contact angle and wettability. Reaction conditions are 3 h at 37.

After showing chemical reaction have the potential to modify electron transport layers, it was important to determine if chemical installation is compatible with OLED processing and operation. Bottom-emitting OLEDs were constructed with the following layer structure: ITO (130 nm) / TCTA: MoO_3 (150 nm, 9 vol%) / TCTA (20 nm) / CBP: $Ir(ppy)_3$ (10 nm, 7 vol %) / TPBi (60 nm) / LiF (1 nm) / Al (100 nm). The reaction was included in the process by removing devices from the evaporator after deposition of TPBi and exposing them to 10 µL of propylene oxide for three hours at 37 before completing the device. During this time, unreacted control devices were left in the glovebox. Both sets were tested for current density and luminance (Figure 6a and b). The measurements show the control and reacted samples have similar turn-on voltages, with the reacted devices showing reduced current and luminance after turn-on. This reduction may not be intrinsic to the reaction and may reflect exposure of TPBi to ambient during the reaction process. No impact is observed on the electroluminescence spectrum (Figure S7), and both devices show similar peak external quantum efficiencies and efficiency roll-off characteristics (Figure 6c). This further suggests that exposure to propylene oxide does not adversely impact the electron-hole charge balance in the device.

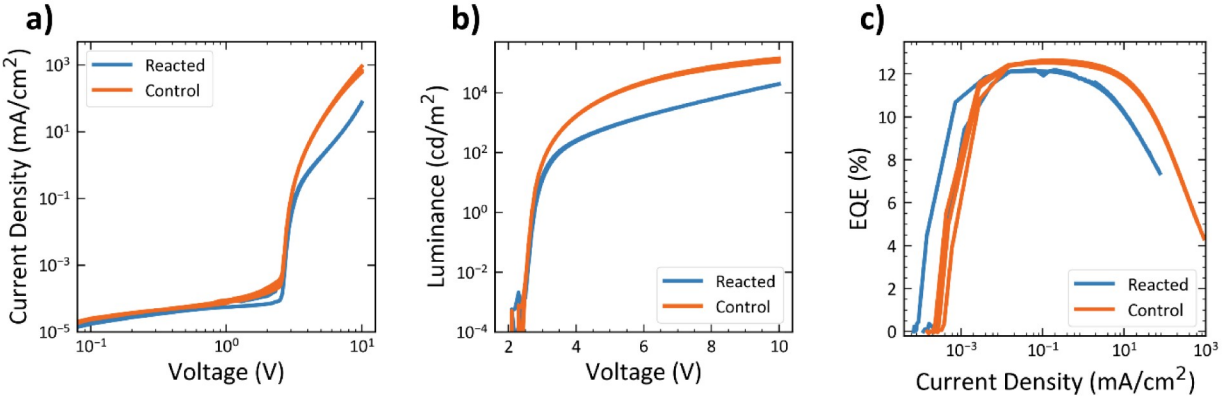

Figure 6. (a) Current density-voltage, (b) luminance-voltage, and (c) the external quantum efficiency-current density characteristics for reacted (blue) and unreacted (orange) OLEDs.

4. Conclusion.

In summary, we have developed and characterized a reaction between TPBi and propylene oxide to show chemical installation is a viable method for installing adlayers on ETLs. EDX and high-resolution XPS indicate a controllable 1-3 nm thick layer of propylene oxide remains on the surface of TPBi. SEM imaging shows the integrity of the thin film is maintained for device compatibility when the reaction is held to milder conditions. Exposing a bottom-emission OLED device to the mild propylene oxide reaction results in no serious damage and no significant negative effects on the device's functionality. This reaction provides evidence that chemically installed adlayers are possible on common ETLs and shows a new route of surface modifications of TPBi that can address the problems surrounding modern OLEDs and ETLs.

CRediT authorship contribution statement

Kevin C. DePope: Investigation, Formal Analysis, Visualization, Writing - Original Draft **Siliang He:** Investigation, Writing - Review & Editing **Yicheng Liu:** Investigation, Writing - Review & Editing **Evgeny Pakhomenko:** Investigation, Formal Analysis, Visualization, Writing - Review & Editing **Russell J. Holmes:** Conceptualization, Methodology, Supervision, Funding Acquisition, Writing - Review & Editing **Jacob W. Ciszek:** Conceptualization, Methodology, Supervision, Funding Acquisition, Writing - Review & Editing

Declaration of competing interest

The authors declare that they have no known competing financial interests or personal relationships that could have appeared to influence the work reported in this paper.

Data availability

Data will be made available upon request.

Declaration of Generative AI and AI-assisted technologies in the writing process

No use of AI or AI-assisted technologies was used during the preparation of this work.

Supplementary Information

Electronic supplementary information (ESI) available: Equations and calculations, ImageJ processing images, additional SEM images, mild temperature table, and additional OLED testing. See DOI:

Acknowledgments

J.W.C. gratefully acknowledges financial support from the National Science Foundation (NSF), no. 1956202. RJH acknowledges support from NSF award 2016450, Ronald L. and Janet A. Christenson, and the University of Minnesota Sundahl Fellowship. This work made use of instruments in the Electron Microscopy Core of UIC's Research Resources Center.

References

[1] Xie, J.; Li, P.; Ho, K.; Walker, G. C.; Lu, Z. Effect of Ag Cathode Deposition Rate on the Performance of Organic Light-Emitting Diodes. *Mater. Sci. Semicond. Process.* 117 (2020)

105170. https://doi.org/10.1016/j.mssp.2020.105170.
[2] Shin, H. Y.; Suh, M. C. Effect of the Thermal Evaporation Rate of Al Cathodes on Organic Light Emitting Diodes. *Mater. Sci. Eng. B* 188 (2014) 8–12. https://doi.org/10.1016/j.mseb.2014.05.013.
[3] Angel, F. A.; Wallace, J. U.; Tang, C. W. Effect of Lithium and Silver Diffusion in Single-Stack and Tandem OLED Devices. *Org. Electron.* 42 (2017) 102–106. https://doi.org/10.1016/j.orgel.2016.12.023.
[4] Gil, T. H.; May, C.; Scholz, S.; Franke, S.; Toerker, M.; Lakner, H.; Leo, K.; Keller, S. Origin of Damages in OLED from Al Top Electrode Deposition by DC Magnetron Sputtering. *Org. Electron.* 11 (2010) 322–331. https://doi.org/10.1016/j.orgel.2009.11.011.
[5] Janssen, F. J. J.; Van Ijzendoorn, L. J.; Denier Van Der Gon, A. W.; De Voigt, M. J. A.; Brongersma, H. H. Interface Formation between Metal and Poly-Dialkoxy-p-Phenylene Vinylene. *Phys. Rev. B - Condens. Matter Mater. Phys.* 70 (2004) 1–11. https://doi.org/10.1103/PhysRevB.70.165425.
[6] Song, M. G.; Kim, K. S.; Yang, H. I.; Kim, S. K.; Kim, J. H.; Han, C. W.; Choi, H. C.; Pode, R.; Kwon, J. H. Highly Reliable and Transparent Al Doped Ag Cathode Fabricated Using Thermal Evaporation for Transparent OLED Applications. *Org. Electron.* 76 (2020) 105418. https://doi.org/10.1016/j.orgel.2019.105418.
[7] Tomita, Y.; Park, T. uk; Nakayama, T. Metal-Atom Interactions and Clustering in Organic Semiconductor Systems. *J. Electron. Mater.* 46 (2017) 3927–3932. https://doi.org/10.1007/s11664-016-5090-4.
[8] Cho, J. H.; Kim, D. H.; Jang, Y.; Lee, W. H.; Ihm, K.; Han, J. H.; Chung, S.; Cho, K. Effects of Metal Penetration into Organic Semiconductors on the Electrical Properties of Organic Thin Film Transistors. *Appl. Phys. Lett.* 89 (2006) 132101. https://doi.org/10.1063/1.2357155.
[9] Scholz, S.; Kondakov, D.; Lussem, B.; Leo, K. Degradation Mechanisms and Reactions in Organic Light-Emitting Devices. *Chem. Rev.* 115 (2015) 8449–8503. https://doi.org/10.1021/cr400704v.
[10] Wang, M.; Xie, F.; Du, J.; Tang, Q.; Zheng, S.; Miao, Q.; Chen, J.; Zhao, N.; Xu, J. B. Degradation Mechanism of Organic Solar Cells with Aluminum Cathode. *Sol. Energy Mater. Sol. Cells* 95 (2011) 3303–3310. https://doi.org/10.1016/j.solmat.2011.07.020.
[11] Turak, A. Interfacial Degradation in Organic Optoelectronics. *RSC Adv.* 3 (2013) 6188–6225. https://doi.org/10.1039/c2ra22770c.
[12] Zilberberg, K.; Meyer, J.; Riedl, T. Solution Processed Metal-Oxides for Organic Electronic Devices. *J. Mater. Chem. C* 1 (2013) 4796–4815. https://doi.org/10.1039/c3tc30930d.
[13] Izawa, S.; Hashimoto, K.; Tajima, K. Surface Functionalization of Organic Semiconductor Films by Segregated Monolayers. *Phys. Chem. Chem. Phys.* 16 (2014) 16383–16387. https://doi.org/10.1039/c4cp02305f.
[14] Moulé, A. J.; Jung, M. C.; Rochester, C. W.; Tress, W.; Lagrange, D.; Jacobs, I. E.; Li, J.; Mauger, S. A.; Rail, M. D.; Lin, O.; Bilsky, D. J.; Qi, Y.; Stroeve, P.; Berben, L. A.; Riede, M. Mixed Interlayers at the Interface between PEDOT:PSS and Conjugated Polymers Provide Charge Transport Control. *J. Mater. Chem. C* 3 (2015), 2664–2676. https://doi.org/10.1039/c4tc02251c.
[15] Wu, H. R.; Song, Q. L.; Wang, M. L.; Li, F. Y.; Yang, H.; Wu, Y.; Huang, C. H.; Ding, X. M.; Hou, X. Y. Stable Small-Molecule Organic Solar Cells with 1,3,5-Tris(2-N-Phenylbenzimidazolyl) Benzene as an Organic Buffer. *Thin Solid Films* 515 (2007) 8050–8053. https://doi.org/10.1016/j.tsf.2007.03.187.

[16] Lassiter, B. E.; Wei, G.; Wang, S.; Zimmerman, J. D.; Diev, V. V.; Thompson, M. E.; Forrest, S. R. Organic Photovoltaics Incorporating Electron Conducting Exciton Blocking Layers. *Appl. Phys. Lett.* 98 (2011) 243307. https://doi.org/10.1063/1.3598426.
[17] Seol, Y. G.; Lee, N.; Park, S. H.; Bae, J. Y. Improvement of Mechanical and Electrical Stabilities of Flexible Organic Thin Film Transistor by Using Adhesive Organic Interlayer. *Org. Electron.* 9 (2008) 413–417. https://doi.org/10.1016/j.orgel.2008.02.003.
[18] Lee, H.; Stephenson, J. C.; Richter, L. J.; Mcneill, C. R.; Gann, E.; Thomsen, L.; Park, S.; Jeong, J.; Yi, Y.; Delongchamp, D. M.; Page, Z. A.; Puodziukynaite, E.; Emrick, T.; Briseno, A. L. The Structural Origin of Electron Injection Enhancements with Fulleropyrrolidine Interlayers. *Adv. Mater. Interfaces* 3 (2016) 1500852. https://doi.org/10.1002/admi.201500852.
[19] Jung, J. W.; Jo, J. W.; Jo, W. H. Enhanced Performance and Air Stability of Polymer Solar Cells by Formation of a Self-Assembled Buffer Layer from Fullerene-End-Capped Poly(Ethylene Glycol). *Adv. Mater.* 23 (2011) 1782–1787. https://doi.org/10.1002/adma.201003996.
[20] Hänsel, H.; Zettl, H.; Krausch, G.; Schmitz, C.; Kisselev, R.; Thelakkat, M.; Schmidt, H. W. Combinatorial Study of the Long-Term Stability of Organic Thin-Film Solar Cells. *Appl. Phys. Lett.* 81 (2002) 2106–2108. https://doi.org/10.1063/1.1506203.
[21] Johnson, R. W.; Hultqvist, A.; Bent, S. F. A Brief Review of Atomic Layer Deposition : From Fundamentals to Applications. *Biochem. Pharmacol.* 17 (2014) 236–246. https://doi.org/10.1016/j.mattod.2014.04.026.
[22] Aydin, E.; Altinkaya, C.; Smirnov, Y.; Yaqin, M. A.; Zanoni, K. P. S.; Paliwal, A.; Firdaus, Y.; Allen, T. G.; Anthopoulos, T. D.; Bolink, H. J.; Morales-Masis, M.; De Wolf, S. Sputtered Transparent Electrodes for Optoelectronic Devices: Induced Damage and Mitigation Strategies. *Matter* 4 (2021) 3549–3584. https://doi.org/10.1016/j.matt.2021.09.021.
[23] Huseynova, G.; Lee, J.; Kim, Y. H.; Lee, J. Transparent Organic Light-Emitting Diodes : Advances , Prospects , and Challenges. *Adv. Opt. Mater.* 9 (2021) 2002040. https://doi.org/10.1002/adom.202002040.
[24] Huang, Z.; Zhang, Y.; He, Y.; Song, H.; Yin, C.; Wu, K. A Chemist's Overview of Surface Electron Spins. *Chem Soc Rev* 46 (2017) 1955–1976. https://doi.org/10.1039/c6cs00891g.
[25] Li, F.; Hopwood, J. P.; Galey, M. M.; Sanchez, L. M.; Ciszek, J. W. Chemically Transformed Monolayers on Acene Thin Films for Improved Metal/Organic Interfaces. *Chem. Commun.* 55 (2019) 13975–13978. https://doi.org/10.1039/c9cc07234a.
[26] Ciszek, J. W.; Piranej, S.; Shelhart Sayers, M. A. W.; Deye, G. J.; Maximoff, S. N.; Hopwood, J. P.; Park, H.; Slavsky, J. G. Role of Surface Phenomena in the Reaction of Molecular Solids: The Diels-Alder Reaction on Pentacene. *CrystEngComm* 22 (2020) 4108–4115. https://doi.org/10.1039/d0ce00269k.
[27] Gammon, W. J.; Kraft, O.; Reilly, A. C.; Holloway, B. C. Experimental Comparison of N(1s) X-Ray Photoelectron Spectroscopy Binding Energies of Hard and Elastic Amorphous Carbon Nitride Films with Reference Organic Compounds. *Carbon N. Y.* 41 (2003) 1917–1923. https://doi.org/10.1016/S0008-6223(03)00170-2.
[28] Giesbers, M.; Marcelis, A. T. M.; Zuilhof, H. Simulation of XPS C1s Spectra of Organic Monolayers by Quantum Chemical Methods. *Langmuir* 29 (2013) 4782–4788. https://doi.org/10.1021/la400445s.
[29] Gengenbach, T. R.; Major, G. H.; Linford, M. R.; Easton, C. D. Practical Guides for X-Ray Photoelectron Spectroscopy (XPS): Interpreting the Carbon 1s Spectrum Practical Guides

for x-Ray Photoelectron Spectroscopy (XPS): Interpreting the Carbon 1s Spectrum. *J. Vac. Sci. Technol. A* 39 (2021) 013204. https://doi.org/10.1116/6.0000682.
[30] Holbrey, J. D.; Turner, M. B.; Reichert, W. M.; Rogers, R. D. New Ionic Liquids Containing an Appended Hydroxyl Functionality from the Atom-Efficient, One-Pot Reaction of 1-Methylimidazole and Acid with Propylene Oxide. *Green Chem.* 5 (2003) 731–736. https://doi.org/10.1039/b311717k.
[31] Cooper, G.; Irwin, W. J. 1-Styrylimidazoles. *J. Chem. Soc. Perkin Trans. 1* (1976) 545–549. https://doi.org/10.1039/P19760000545.
[32] Li, F.; Hopwood, J. P.; Hu, X.; Ambagaspitiya, T. D.; Asetre Cimatu, K. L.; Ciszek, J. W. Monolayer-Induced Changes in Metal Penetration and Wetting for Metal-on-Organic Interfaces. *Chem. Mater.* 33 (2021) 9515–9523. https://doi.org/10.1021/acs.chemmater.1c02606.
[33] Borges, B. G. A. L.; Gioti, M.; Correa, R. S.; Andreopoulou, A. K.; Veiga, A. G.; Laskarakis, A.; Kallitsis, K.; Logothetidis, S.; Rocco, M. L. M. Surface, Interface and Electronic Studies on Anthracene Derived Polymeric Thin Films for OLED Applications. *Opt. Mater.* 117 (2021) 111145. https://doi.org/10.1016/j.optmat.2021.111145.
[34] Chen, J.; Franking, R.; Ruther, R. E.; Tan, Y.; He, X.; Hogendoorn, S. R.; Hamers, R. J. Formation of Molecular Monolayers on TiO 2 Surfaces : A Surface Analogue of the Williamson Ether Synthesis. *Langmuir* 27 (2011) 6879–6889. https://doi.org/10.1021/la2008528
[35] Chen, J.; Ruther, R. E.; Tan, Y.; Bishop, L. M.; Hamers, R. J. Molecular Adsorption on ZnO($10\bar{1}0$) Single-Crystal Surfaces: Morphology and Charge Transfer. *Langmuir* 28 (2012) 10437–10445. https://doi.org/10.1021/la301347t.
[36] Bangsund, J. S.; Fielitz, T. R.; Steiner, T. J.; Shi, K.; Van Sambeek, J. R.; Clark, C. P.; Holmes, R. J. Formation of Aligned Periodic Patterns during the Crystallization of Organic Semiconductor Thin Films. *Nat. Mater.* 18 (2019) 725–731. https://doi.org/10.1038/s41563-019-0379-3.
[37] Calimano, J.; Pinero-Cruz, D. M.; Fielitz, T. R.; Holmes, R. J.; Li, F.; Florian, J.; Ciszek, J. W. Solid-State Properties and Spectroscopic Analysis of Thin-Film TPBi´ ,. *J. Phys. Chem. C* 124 (2020) 23716–23723. https://doi.org/10.1021/acs.jpcc.0c06959.
[38] Herzberger, J.; Niederer, K.; Pohlit, H.; Seiwert, J.; Worm, M.; Wurm, F. R.; Frey, H. Polymerization of Ethylene Oxide , Propylene Oxide , and Other Alkylene Oxides : Synthesis , Novel Polymer Architectures , and Bioconjugation. *Chem. Rev.* 116 (2016) 2170–2243. https://doi.org/10.1021/acs.chemrev.5b00441.